

Vibration eigenmodes of the Au-(5 × 2)/Si(111) surface studied by Raman spectroscopy and first-principles calculations

M. Liebhaber, B. Halbig,* U. Bass, and J. Geurts

Experimentelle Physik 3, Physikalisches Institut, Universität Würzburg, Am Hubland, 97074 Würzburg, Germany

S. Neufeld, S. Sanna, and W. G. Schmidt

Department Physik, Universität Paderborn, Warburger Strasse 100, 33098 Paderborn, Germany

E. Speiser, J. Räthel, S. Chandola, and N. Esser

Leibniz-Institut für Analytische Wissenschaften-ISAS-e.V., Schwarzschildstrasse 8, 12489 Berlin, Germany

(Received 13 October 2016; revised manuscript received 21 November 2016; published 19 December 2016)

Ordered submonolayers of adsorbate atoms on semiconductor surfaces constitute a playground for electronic correlation effects, which are tightly connected to the local atomic arrangement and the corresponding vibration eigenmodes. We report on a study of the vibration eigenmodes of Au-covered Si(111) surfaces with (5 × 2) reconstruction using polarized Raman spectroscopy and first-principles calculations. Upon Au coverage, the vibration eigenmodes of the clean reconstructed Si(111)-(7 × 7) surface are quenched and replaced by new eigenmodes, determined by the Au-(5 × 2) reconstruction. Several polarization-dependent surface eigenmodes emerge in the spectral range from 25 to 120 cm⁻¹, with the strongest ones at 29, 51, and 106 cm⁻¹. In our first-principles calculations we have determined the vibration frequencies, the corresponding elongation patterns, and the Raman intensities for two different structure models currently discussed in the literature. The best agreement with the experimental results is achieved for a model with 0.7 monolayer coverage and seven Au atoms per unit cell, proposed by S. G. Kwon and M. H. Kang [*Phys. Rev. Lett.* **113**, 086101 (2014)].

DOI: [10.1103/PhysRevB.94.235304](https://doi.org/10.1103/PhysRevB.94.235304)

I. INTRODUCTION

Ordered (sub)monolayers on semiconductor surfaces, e.g., one-dimensional metallic chains, have received a great deal of attention as model systems for low-dimensional physics and electron correlation effects [1].

A possible realization is the material system Au/Si(111), where, depending on the Au coverage and the substrate temperature, one- or two-dimensional ordered Au patterns can be achieved, whose reconstructions are characterized by the (5 × 2) and ($\sqrt{3} \times \sqrt{3}$) periodicity, respectively [2,3].

The Au-(5 × 2)/Si(111) reconstruction with its one-directional Au-induced chains has been the subject of extended experimental and theoretical investigations [4–11] for many years. In spite of all these studies, the atomic arrangement of this reconstruction has given rise to recent disputes in the literature. Erwin, Barke, and Himpsel established a model, based on a Au coverage of 0.6 monolayer (ML), resulting in a surface unit cell consisting of 6 Au atoms and 12 top-layer Si atoms, leading to an arrangement of Au triple chains and Si honeycomb chains [5]. This reconstruction, in the following denoted as the EBH model, is depicted in Fig. 1(a). In order to match this intrinsically (5 × 1)-periodic model with the experimental (5 × 2) result from low-energy electron diffraction (LEED) [12], a (5 × 4) decoration by Si adatoms was invoked, which induces within the Au double chains a dimerization with an alternating in-plane tilt, resulting in a doubled periodicity along the chain direction. The Au chains are metallic, leading to a pronounced one-dimensional surface conductivity. This model was questioned by Abukawa

and Nishigaya [6]. To explain reflection high-energy electron diffraction (RHEED) and scanning tunneling microscopy (STM) results, they excluded the existence of Si honeycomb chains and claimed Y-shaped structures of six Au atoms (Eiffel Tower model). However, the latter model was ruled out by Hogan *et al.* [7] for reasons of energetic instability due to its high formation energy according to density-functional theory (DFT) calculations and incompatibility with experimental results from reflectance anisotropy spectroscopy (RAS). The same conclusion was obtained from calculated band structures and scanning tunneling images by Seino and Bechstedt [9]. In the most recent model, proposed by Kwon and Kang [8] and displayed in Fig. 1(b), the EBH model is slightly modified by invoking a Au coverage of 0.7 ML with one additional Au atom in each unit cell, which results in a more favorable energy [difference from the EBH model of 0.92 eV per (5 × 2) unit cell], an improved compatibility with the STM images, and an intrinsic (5 × 2) periodicity. The latter model will be referred to as the KK model. It was favored by several recent studies, employing surface-x-ray diffraction [10], DFT calculations of the core-level shifts in x-ray photoemission spectroscopy (XPS) [13], and comparative hybrid DFT calculations of atomic structure, electronic band structure, and reflectance anisotropy [14]. Furthermore, it should also be noted that the equilibrium surface has ≈ 0.025 -ML coverage of Si adatoms, divided into structural domains without adatoms and domains with ≈ 0.05 -ML Si adatom coverage. These Si adatoms, which are not shown in the structural models in Fig. 1, have been verified by several research groups [5,14–16].

Besides the above-mentioned surface analysis techniques, another very sensitive experimental test for models of the atomic structure and, moreover, of the bonding of adsorbates is provided by the analysis of their lattice dynamics. Therefore,

*benedikt.halbig@physik.uni-wuerzburg.de

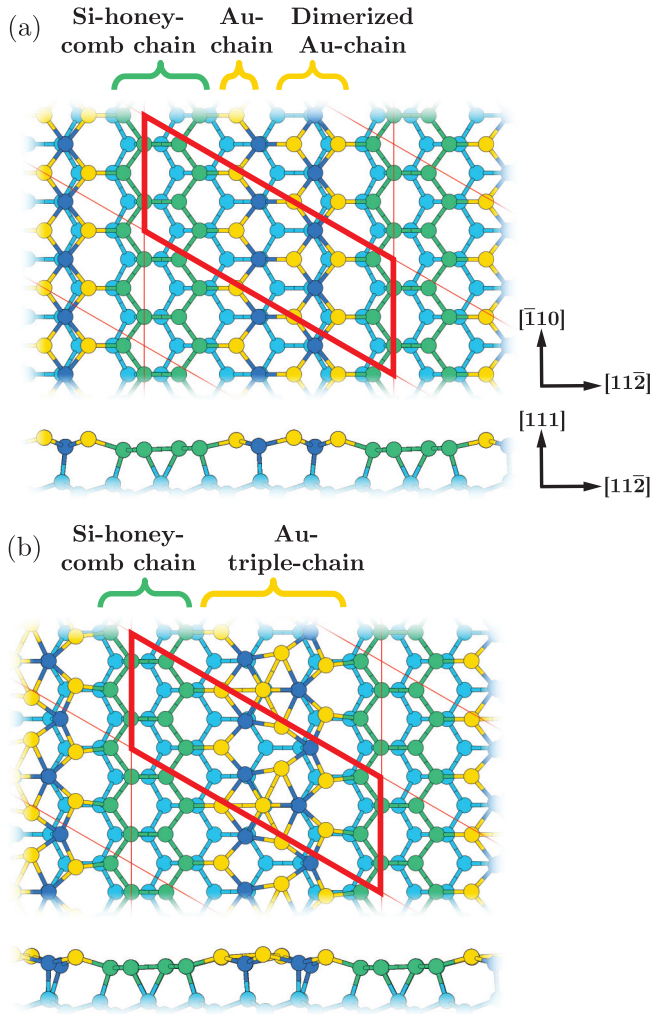


FIG. 1. Structural models of the Au/Si(111)Au surface within (a) the EBH model (0.6-ML coverage) [5] and (b) the KK model (0.7-ML coverage) [8]. Yellow balls represent gold atoms, while green and dark blue balls identify the Si honeycomb chain and the remaining Si surface atoms, respectively. Si atoms of the underlying bulk layer are colored light blue. The (5×2) surface unit cell is outlined in red. Si adatoms are not included.

in this study we focus on the dynamical properties of the Au/Si(111) surface with (5×2) reconstruction, determined by surface Raman spectroscopy (SRS). In recent years, this optical technique, traditionally widely used for investigating phonons in semiconductor bulk and multilayer systems [17,18], has advanced to a sensitive probe for vibration eigenmodes of clean surfaces as well as ordered adsorbed (sub)monolayers [19–28], although the Raman intensity of surface and adsorbate vibrations is expected to be far below the intensity of bulk substrate vibrations. As a major advantage it provides a high spectral resolution in the range of 1 cm^{-1} . In addition, when utilizing polarized Raman scattering, the dependence on the directions \vec{e}_i and \vec{e}_s of the electric fields of the incoming and scattered light reveals the vibration symmetry properties through the Raman tensors [29,30]. The Au- (5×2) reconstruction on Si(111) is highly anisotropic, and a glide reflection plane within the surface exists as the only

symmetry element. This refers to a pg two-dimensional space group (according to the C_s three-dimensional point group) giving rise to diagonal (A') and off-diagonal (A'') Raman tensors. Thus, the Raman scattering cross section is expected to show a significant dependence on polarization of incident and scattered light.

In this paper, we report on the observation of vibration eigenmodes of Au-covered Si(111) surfaces with (5×2) reconstruction using polarized *in situ* SRS under UHV conditions. The mode assignment is performed by means of first-principles calculations of the surface dynamics. After a survey of the sample preparation procedure, the experimental setup, and the calculation methodology, the results are presented. Starting with a brief presentation of LEED results for the identification of the reconstruction pattern and as proof of the sample preparation quality, subsequently, the *in situ* surface Raman spectra are discussed with special reference to the distinction between the net Au-induced signatures and the intense background from Si bulk contributions. Finally, the obtained Au-induced Raman signatures are correlated with results from first-principles calculations, which derive the vibration frequencies, elongation patterns, and Raman intensities of the Au-induced eigenmodes for the EBH and KK models. Although these calculations for practical reasons do not imply the different domains and the related Si adatoms, they allow for a comparison of these two models.

II. EXPERIMENT AND CALCULATION METHODOLOGY

The sample substrates were prepared from commercially available Si(111) wafers with a miscut angle between 0.5° and 1.0° . For the preparation of the (7×7) surface reconstruction, the samples were initially pretreated in an *ex situ* wet-chemical cleaning procedure, followed by an *in situ* flash-annealing process. Further details of the Si(111)- (7×7) surface preparation are described elsewhere [27]. For preparing the Au- (5×2) reconstruction, ≈ 1.5 ML of Au were deposited at $T_{\text{sub}} = 950 \text{ K}$, followed by repeated annealing steps at $T_{\text{sub}} \approx 1050 \text{ K}$.

In order to study the Au/Si(111) vibration modes, *in situ* SRS under UHV conditions ($p < 1 \times 10^{-10}$ mbar) was performed in a near-backscattering geometry (angle of incidence of 60°), directly attached to the UHV system. In order to validate the reproducibility and exclude possible setup artifacts, these Raman measurements were performed twice, using two different setups with distinct high-sensitivity spectrometer types, a triple DILOR-XY and a SPEX 1403 double monochromator, both with a very efficient rejection of the elastically scattered laser light and equipped with high-efficiency Si-based charge-coupled device detectors (ANDOR iDus series). The light source was a solid-state laser with a photon energy of 1.87 eV ($\approx 660 \text{ nm}$).

For the analysis of the symmetry properties of the vibration modes, the spectra were taken with well-defined polarization directions of the incoming and outgoing light. They are labeled according to the well-established Porto notation [30,31]: backscattering from a z -oriented surface with incoming polarization direction e_i and outgoing e_s is denoted as $z(e_i e_s)\bar{z}$. Thus, the configurations $z(xx)\bar{z}$ and $z(yy)\bar{z}$ give access to the A' modes through the Raman tensor elements α_{xx} and α_{yy} , respectively, while the tensor element $\alpha_{xy} = \alpha_{yx}$ of the

A'' modes can be probed in the configurations $z(xy)\bar{z}$ and $z(yx)\bar{z}$.

Vibrational properties of the Au-(5 × 2)/Si(111) surface were additionally investigated by first-principles calculations within the DFT. To this end, the phononic displacement patterns as well as the Raman spectra of both the KK and EBH models were evaluated within (5 × 2) slabs containing seven bilayers of Si in addition to the reconstructed surface on top (see Fig. 1). The slabs also contained a layer of hydrogen passivation atoms and a vacuum region with a thickness of 20 Å. The outer three substrate bilayers (i.e., six Si layers) and all the termination atoms are allowed to relax freely (force threshold of 0.01 eV/Å), while the remaining atoms are kept fixed at the bulk positions.

In order to investigate the Raman spectra of both systems, the differential scattering efficiency with respect to the collection angle Ω was evaluated with the same formalism as employed in Ref. [32]. It is defined as [30,33]

$$\frac{dS^m}{d\Omega} = \frac{(\omega_i - \omega_m)^4}{(4\pi)^2 c^4} |\vec{e}_i \cdot \underline{\underline{\alpha}}^m \cdot \vec{e}_s|^2 \frac{\hbar}{2\omega_m} (n_m + 1). \quad (1)$$

Here, ω_i and \vec{e}_i denote the frequency and polarization vector of an incident photon, which is scattered into a photon with frequency $\omega_s \equiv \omega_i - \omega_m$ and polarization vector \vec{e}_s , creating a phonon mode m with frequency ω_m in the process. n_m indicates the temperature-dependent phononic particle number given by the Bose-Einstein distribution. Both optical and vibrational properties of the system enter the equation via the Raman susceptibility tensor $\underline{\underline{\alpha}}^m$,

$$\alpha_{ij}^m = \frac{\partial \chi_{ij}}{\partial \xi^m}, \quad (2)$$

where the normal-mode displacement and linear dielectric susceptibility tensor are expressed by ξ and χ_{ij} , respectively. The latter is calculated within the Perdew, Burke, and Ernzerhof (PBE) parametrization of the generalized gradient approximation (GGA) [34] as implemented in the Vienna Ab initio Simulation Package (VASP) [35] using a $4 \times 12 \times 1$ k -point mesh and a 500 eV plane-wave cutoff energy. The evaluation of the derivative in Eq. (2) is carried out by finite difference differentiation of the optical dielectric function with respect to ξ^m . The dielectric function is calculated within the independent particle approximation [36]. The total number of considered bands was tested regarding the convergence of the dielectric function. It was found that the function is reproduced with an error <1% for 800 bands. The normal mode displacement patterns were evaluated via the frozen-phonon approach [37]. Each mode is furthermore artificially broadened by a Lorentzian function with an arbitrary width of 5 cm⁻¹ for the construction of theoretically calculated Raman spectra. Obviously, the Raman cross section depends on the excitation energy [see Eq. (2)]. This needs to be taken into account in the comparison of experimental and calculated Raman spectra.

III. RESULTS AND DISCUSSION

A. LEED analysis

Prior to the Raman spectroscopy experiments, the LEED pattern of the Au/Si(111) samples was recorded for verification

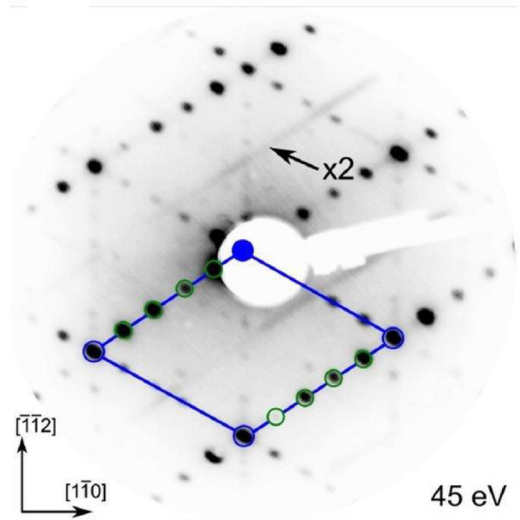


FIG. 2. The (5 × 2) LEED pattern recorded at an electron energy of 45 eV. The green circles on the edges of the blue (1 × 1) rhomb indicate the superstructure reflexes. Together with the streaks, marked by the arrow labeled “x2,” they document the (5 × 2) superstructure.

of the quality of the interface ordering and, moreover, for the identification of the reconstruction, its purity in terms of (5 × 2) vs ($\sqrt{3} \times \sqrt{3}$) reconstruction, the distribution of domain orientations, and the determination of the in-plane crystal directions ($[11\bar{2}]$ and $[\bar{1}10]$) as a reference for polarized SRS.

Figure 2 shows the LEED pattern obtained at 300 K, with an electron energy of 45 eV from the (5 × 2)-reconstructed Au/Si(111) surface, prepared by the flash-annealing process described above. The blue rhomb denotes the (1 × 1) unit cell. The high-quality Au-(5 × 2) periodicity in real space is reflected in the LEED pattern by the four sharp equidistant superstructure spots along one main axis (circled in Fig. 2) and the superstructure signatures (marked as ×2), which are centered between the main peaks along the complementary axis and are rather blurry along the direction perpendicular to this axis. Together, these two types of superstructure spots indicate a high correlation along the chains and a much weaker chain-to-chain correlation.

Furthermore, the threefold symmetry of Si(111) is broken since one domain orientation clearly dominates. Reflectance anisotropy spectroscopy [7] allows a quantitative assessment and yields in this case an abundance of 75% for the main domain orientation. The preferential orientation of the Au chains along one direction will allow us in polarized Raman scattering to distinguish between the diagonal Raman tensor elements parallel and perpendicular to the chains.

B. UHV Raman spectra of Au-(5 × 2)/Si(111)

In the search for vibration modes of the Au-(5 × 2) reconstruction, Raman spectra with different polarization configurations were recorded *in situ* in UHV, immediately after the flash-annealing preparation of this reconstruction and, for comparison, subsequently also after accelerated aging of the surface by exposure to a substantially increased base pressure of the residual gas ($p \approx 10^{-8}$ mbar) for more than 10 min. The parameters of this aging procedure were chosen such that

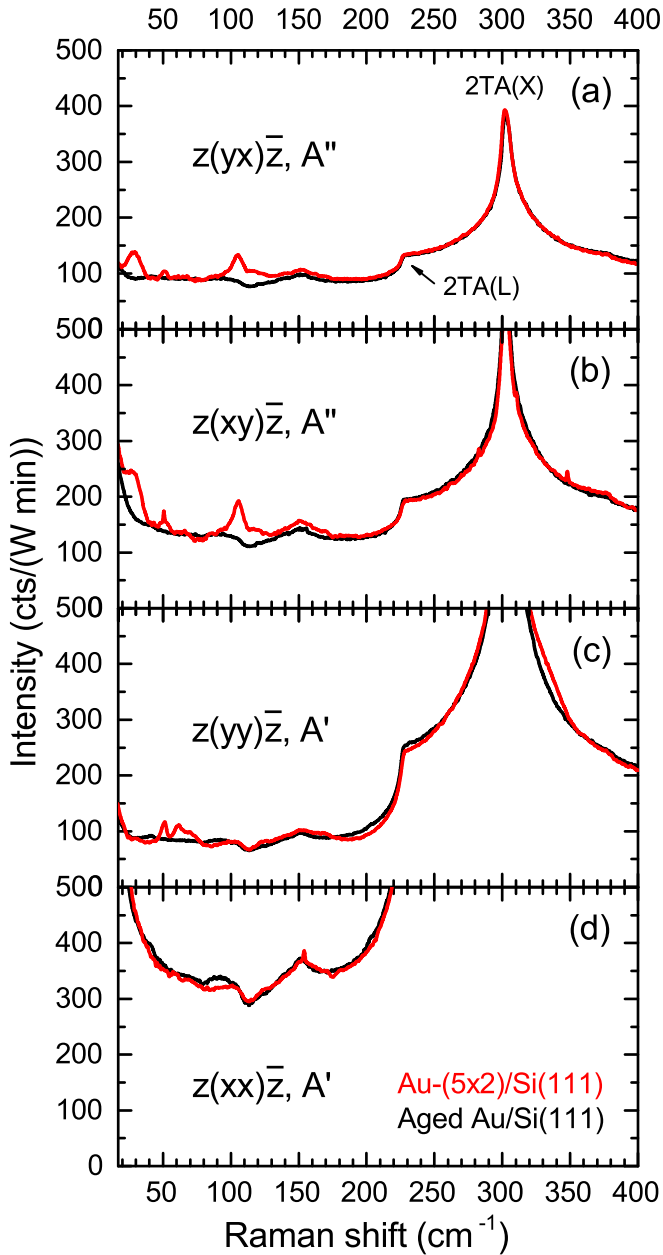


FIG. 3. Polarized Raman spectra of Au-(5 × 2)/Si(111) (red) and the aged Au/Si(111) surface (black). Polarization configurations are (a) $z(yx)\bar{z}$, (b) $z(xy)\bar{z}$, (c) $z(yy)\bar{z}$, and (d) $z(xx)\bar{z}$, where x is the Au-chain direction ($1\bar{1}0$). Excitation wavelength is 660 nm, and temperature is 300 K.

the residual gas dose is in the range of 10 langmuirs. This is just sufficient for eliminating the Au-(5 × 2) reconstruction, as evidenced by the fading of the corresponding LEED pattern, but without further chemical impact for the Si substrate.

The polarized spectra were recorded for the full set of polarization configurations, i.e., $z(yx)\bar{z}$, $z(xy)\bar{z}$, $z(yy)\bar{z}$, and $z(xx)\bar{z}$, with the x axis along the Au-chain direction ($1\bar{1}0$) of the dominant domain and the y axis perpendicular to these chains. The resulting spectra are shown in Figs. 3(a) to 3(d).

Because the light penetration depth in Si at 660 nm amounts to $\approx 3\ \mu\text{m}$ [38], the signatures from surfaces and

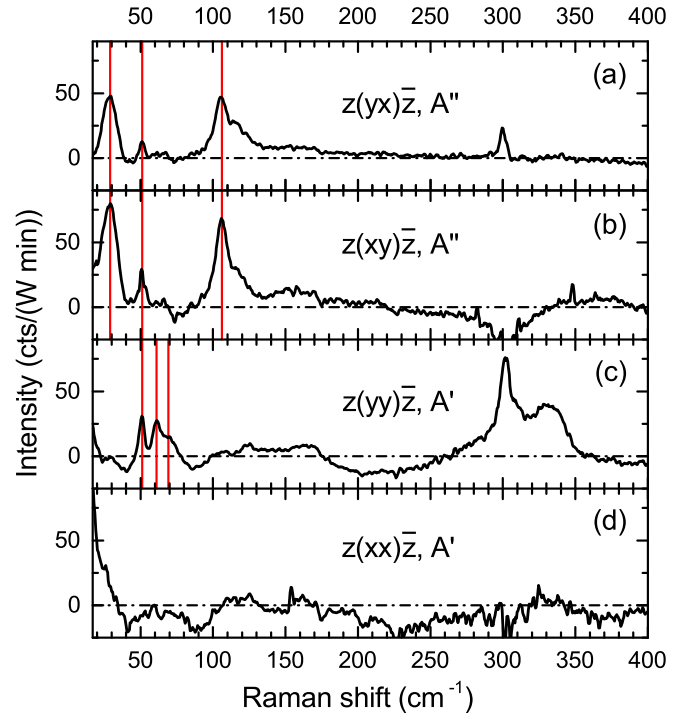


FIG. 4. Intensity difference between the Raman spectra of the Au-(5 × 2)/Si(111) reconstruction and the aged case in Fig. 3, yielding the Au-(5 × 2)-induced vibration modes. Polarization configurations are (a) $z(yx)\bar{z}$, (b) $z(xy)\bar{z}$, (c) $z(yy)\bar{z}$, and (d) $z(xx)\bar{z}$, where x is the Au-chain direction ($1\bar{1}0$).

adsorbates are always superimposed by dominant bulk features in the Raman spectra. In the case of Si, the strongest bulk feature by far originates from the degenerate TO and LO zone-center phonon, denoted as LTO(Γ), located at $521\ \text{cm}^{-1}$ (not shown here). Furthermore, a broadly structured second-order bulk-vibrational Raman signature appears with much lower intensity ($\approx 10^{-2} I_{\text{LTO}}$). This gives rise to the strongest structures in Fig. 3. It consists of a clear peak located at $303\ \text{cm}^{-1}$, originating from second order transverse acoustic phonon scattering (2TA) at the X point of the Brillouin zone and a steplike structure at $230\ \text{cm}^{-1}$ from 2TA at the L point [39–41]. The 2TA(X) peaks clearly dominate in Figs. 3(a) and 3(b), i.e., for the polarization configurations (xy) and (yx), while they even strongly exceed the vertical scaling in Figs. 3(c) and 3(d) because they essentially appear in the polarization configurations (yy) and (xx).

The features of interest in our study, i.e., the vibration modes which are induced by the Au-(5 × 2) reconstruction, appear as the intensity difference between the reconstructed surface (red curves) and the aged one (black curves) in Figs. 3(a)–3(d). These difference spectra are shown in Figs. 4(a)–4(d). Although these features are much weaker (intensities $\approx 10^{-4} I_{\text{LTO}}$), distinct peaks can be identified. These peaks are clearly different from the vibrations of clean Si(111)-(7 × 7) [27] and are attributed to the Au-(5 × 2) reconstruction.

Several polarization-dependent low-frequency Au-induced vibration eigenmodes emerge in the spectral range from 25 to $120\ \text{cm}^{-1}$. Obviously, the difference spectra for the two polarization configurations $z(xy)\bar{z}$ and $z(yx)\bar{z}$, i.e., for

off-diagonal A'' Raman tensors, are quite similar. They show the strongest peaks, located at 29, 51, and 106 cm^{-1} . The A' configuration $z(yy)\bar{z}$ yields a structure between 50 and 80 cm^{-1} , consisting of peaks at 51 and 61 cm^{-1} and a shoulder at 69 cm^{-1} , while no Au-induced contribution is observed for the A' configuration $z(xx)\bar{z}$. The structures, which appear in the difference spectra in the range of the 2TA(X) peak at about 300 cm^{-1} [especially in Fig. 4(c)], are considered artifacts due to the strong sensitivity of the difference intensity at this strong and steep peak to slight relative intensity variations in the individual spectra. Further very small changes of the Raman baseline by surface modification are visible as weak, broad negative features around 50–100 and 200–250 cm^{-1} . We attribute these modifications to surface-activated Raman scattering at bulk Si acoustic phonon modes which is influenced by the surface modification as well, as was observed also for III–V compounds [42].

For each vibration mode the observed peak intensities in the polarized Raman spectra give access to the diagonal A' Raman tensor element R_{yy} perpendicular to the x -directed Au chains and to the off-diagonal A'' elements R_{yx} and R_{xy} . This allows us to correlate them with the results of first-principles model calculations, as described in the following section.

C. First-principles calculations

The comparison of the calculated Raman spectra with the experimental ones requires great care because the calculated Raman scattering efficiencies of each eigenmode turn out to depend individually and strongly on the chosen excitation wavelength. This dependence is a consequence of the frequency-dependent dielectric function. Therefore, the excitation energy in the calculation has to be chosen appropriately for matching the dielectric function at the experimental laser wavelength. For the right choice it has to be considered that DFT band structures typically underestimate the band gap of the underlying Si substrate by an amount of about 0.5 eV [43]; that is, the spectral dependence of the calculated dielectric function is redshifted by this amount with respect to the experimental one. In order to account approximately for this effect we rigidly shift the eigenvalues as done in previous RAS calculations (see, e.g., Ref. [7]). Therefore, all theoretical Raman spectra are evaluated at an excitation energy of 1.38 eV in order to match the dielectric function at the experimental excitation energy of 1.88 eV (laser wavelength 660 nm). The experimental and theoretical Raman spectra of the Au-(5 × 2)/Si(111) reconstruction are compiled in Fig. 5.

Furthermore, when relating theoretical Raman spectra to experimental ones, one has to consider that the theoretical approach does not model the precise experimental setup, i.e., the measurement of the difference between the spectra of the gold-covered and oxidized Si(111) surface. In contrast, the present calculations are performed for Raman spectra of surface localized phonon modes of the Au/Si(111) surface. Also, due to computational limitations, quasiparticle and excitonic effects had to be neglected in the present approach [43]. A further limitation is the omission of the Si adatoms.

Regarding the observation of the A' modes in (yy) polarization, i.e., perpendicular to the chains, the experimentally

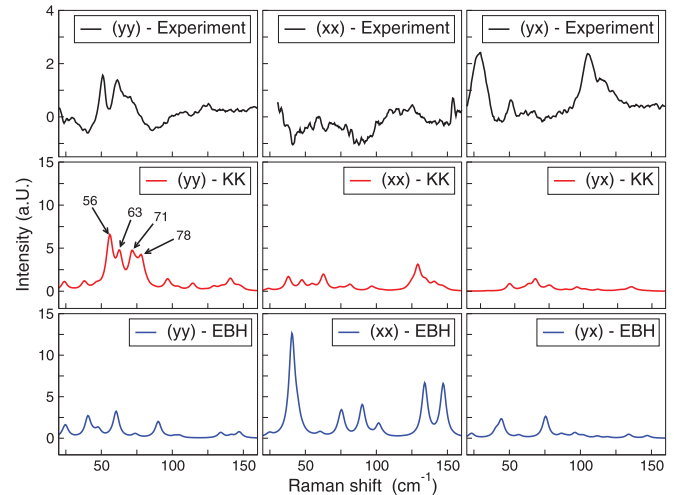


FIG. 5. Measured difference spectra of the Au-(5 × 2)/Si(111) reconstruction (black) along with the calculated Raman spectra within the KK and EBH models (red and blue, respectively). The spectra are depicted within the polarization configurations (yy), (xx), and (yx), which is equivalent to (xy). The intensity scales (in arbitrary units) are equal within each row.

observed peaks between 50 and 80 cm^{-1} are well reproduced within the KK model in terms of peak positions as well as relative intensities. The displacement patterns of the four most dominant theoretical signals, located at 56, 63, 71, and 78 cm^{-1} , are depicted in Fig. 6. They can be assigned to the three experimental peaks at 51, 61, and 69 cm^{-1} , as seen in Fig. 4. All four modes are localized primarily at the gold atoms. Moreover, two modes (56 and 78 cm^{-1}) show displacement patterns primarily perpendicular to the chain

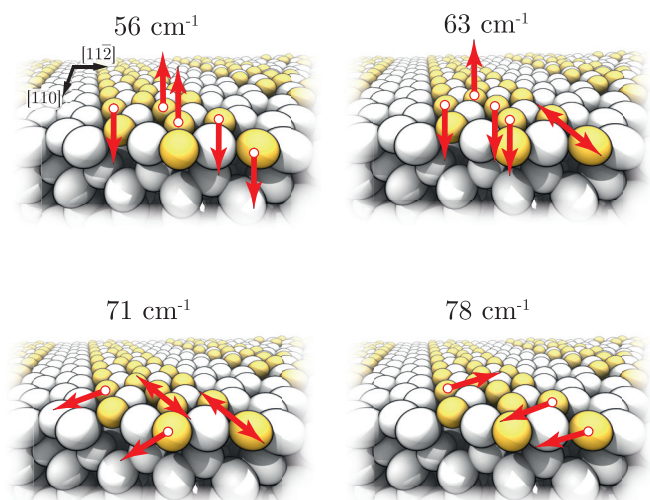


FIG. 6. Schematic displacement patterns of the most dominant phonon modes within the (yy) polarization of the KK model, corresponding to the theoretical Raman peaks in Fig. 5. White and yellow balls represent Si and Au atoms, respectively. Single-headed arrows indicate a rigid translation; double-headed arrows indicate a dimerization motion.

direction $[\bar{1}10]$, while the two remaining modes show no clearly distinguishable orientation.

The experimental A' Raman spectrum within the (xx) polarization, i.e., parallel to the chains, does not show features that can be clearly assigned to phonon modes. This disappearance of the Raman signal agrees much better with the KK model, which should result in only very weak Raman peaks compared to the strong peaks exhibited by the EBH model.

The A'' Raman spectrum in the (yx) polarization, however, reveals significant deviations between experimental and theoretical results in either model. For both models our calculations predict only relatively weak Raman signals, while the experiment features its highest-intensity peaks in this polarization configuration. This may be partially related to the aforementioned limitations of the computational approach. Probably, the fact that features of the experimental (xy) Raman spectra are missing in the calculated one is due to the disregard of the well-established domains and the omission of the associated Si adatoms in our calculations. The fact that in the (yx) Raman spectra features arise which have no counterpart in the calculation would, by implication, result if structural domains distinct from the (5×2) structure discussed so far are sampled as well. This is indeed the case as Si adsorbate atoms have been found on the surface by several groups [5,15,16]. The Si adsorbate atoms were found to allocate in domains which coexist with the pure (5×2) structure which is used for the calculations here. Thus, these Si-adatom-modified domains may give rise to surface vibrational modes which then show up in the Raman spectra of the (5×2) surface in addition to the modes of the KK structure.

This scenario agrees with the experimental observations. Altogether, the present calculations for the KK model agree considerably better with the measured data than the calculations based on the EBH structure. The preference for the KK model is in agreement with experimental results from

surface x-ray diffraction [10], infrared spectroscopy [11], and reflectance anisotropy spectroscopy [14].

IV. SUMMARY

In summary, we have studied the vibration modes of (5×2) -reconstructed Au/Si(111) surfaces by *in situ* polarized Raman spectroscopy experiments in combination with first-principles calculations. Reconstruction-specific Au-induced vibration modes were observed in the spectral range between 25 and 120 cm^{-1} with mode-specific Raman-tensor components. Prominent vibration frequencies for Au- (5×2) are 29 and 106 cm^{-1} with Raman tensor component α_{xy} , 61 and 69 cm^{-1} with Raman tensor component α_{yy} , and 51 cm^{-1} with both tensor components.

Our first-principles-calculated results for the vibration frequencies, the corresponding elongation patterns, and the Raman intensities replicate the experimental Raman spectra to a satisfying degree within the polarization configurations (xx) and (yy) when assuming the atomic structure model by Kwon and Kang [8]. Moreover, Raman spectra suggest the coexistence of different (5×2) structure domains, which could be associated with adatom decoration. The model by Erwin, Barke, and Himpfel [5], on the other hand, features substantial deviations from the measured data within all scattering configurations.

ACKNOWLEDGMENTS

We gratefully acknowledge financial support from the Deutsche Forschungsgemeinschaft in the research units FOR 1162, FOR 1700, project GE 1855/10-2, and projects ES 127/12-1 and SCHM 1361/19. Financial support from the Senatsverwaltung für Wirtschaft, Technologie und Forschung des Landes Berlin, the Ministerium für Innovation, Wissenschaft und Forschung des Landes Nordrhein-Westfalen, and the Bundesministerium für Bildung und Forschung is acknowledged. Moreover, we thank K. M. Wolf for experimental support.

-
- [1] P. C. Snijders and H. H. Weitering, *Rev. Mod. Phys.* **82**, 307 (2010).
- [2] J. Kautz, M. W. Copel, M. S. Gordon, R. M. Tromp, and S. J. van der Molen, *Phys. Rev. B* **89**, 035416 (2014).
- [3] D. Grozea, E. Bengu, and L. Marks, *Surf. Sci.* **461**, 23 (2000).
- [4] J. L. McChesney, J. N. Crain, V. Pérez-Dieste, F. Zheng, M. C. Gallagher, M. Bissen, C. Gundelach, and F. J. Himpfel, *Phys. Rev. B* **70**, 195430 (2004).
- [5] S. C. Erwin, I. Barke, and F. J. Himpfel, *Phys. Rev. B* **80**, 155409 (2009).
- [6] T. Abukawa and Y. Nishigaya, *Phys. Rev. Lett.* **110**, 036102 (2013).
- [7] C. Hogan, E. Ferraro, N. McAlinden, and J. F. McGilp, *Phys. Rev. Lett.* **111**, 087401 (2013).
- [8] S. G. Kwon and M. H. Kang, *Phys. Rev. Lett.* **113**, 086101 (2014).
- [9] K. Seino and F. Bechstedt, *Phys. Rev. B* **90**, 165407 (2014).
- [10] T. Shirasawa, W. Voegeli, T. Nojima, Y. Iwasawa, Y. Yamaguchi, and T. Takahashi, *Phys. Rev. Lett.* **113**, 165501 (2014).
- [11] F. Hötzel, K. Seino, C. Huck, O. Skibbe, F. Bechstedt, and A. Pucci, *Nano Lett.* **15**, 4155 (2015).
- [12] H. Lipson and K. E. Singer, *J. Phys. C* **7**, 12 (1974).
- [13] S. G. Kwon and M. H. Kang, *Phys. Rev. B* **92**, 195301 (2015).
- [14] C. H. Patterson, S. Banerjee, and J. F. McGilp, *Phys. Rev. B* **94**, 165417 (2016).
- [15] I. Barke, S. Polei, V. v. Oeynhausen, and K.-H. Meiwes-Broer, *Phys. Rev. Lett.* **109**, 066801 (2012).
- [16] E. H. Do and H. W. Yeom, *Phys. Rev. Lett.* **115**, 266803 (2015).
- [17] J. Geurts, *Prog. Cryst. Growth Charact. Mater.* **32**, 185 (1996).
- [18] D. Lürßen, A. Dinger, H. Kalt, W. Braun, R. Nötzel, K. Ploog, J. Tümmeler, and J. Geurts, *Phys. Rev. B* **57**, 1631 (1998).
- [19] K. Hinrichs, A. Schierhorn, P. Haier, N. Esser, W. Richter, and J. Sahn, *Phys. Rev. Lett.* **79**, 1094 (1997).
- [20] N. Esser, K. Hinrichs, J. Power, and W. Richter, *Surf. Sci.* **427-428**, 44 (1999).
- [21] N. Esser, *Appl. Phys. A* **69**, 507 (1999).
- [22] *Light Scattering in Solids VIII: Fullerenes, Semiconductor Surfaces, Coherent Phonons*, edited by M. Cardona and G. Güntherodt, Topics in Applied Physics Vol. 76 (Springer, Berlin, 2000).

- [23] K. Fleischer, S. Chandola, N. Esser, W. Richter, and J. F. McGilp, *Phys. Rev. B* **76**, 205406 (2007).
- [24] E. Speiser, S. Chandola, K. Hinrichs, M. Gensch, C. Cobet, S. Wippermann, W. Schmidt, F. Bechstedt, W. Richter, K. Fleischer, J. F. McGilp, and N. Esser, *Phys. Status Solidi B* **247**, 2033 (2010).
- [25] J. Räthel, E. Speiser, N. Esser, U. Bass, S. Meyer, J. Schäfer, and J. Geurts, *Phys. Rev. B* **86**, 035312 (2012).
- [26] V. Wagner, J. Wagner, S. Gundel, L. Hansen, and J. Geurts, *Phys. Rev. Lett.* **89**, 166103 (2002).
- [27] M. Liebhaber, U. Bass, P. Bayersdorfer, J. Geurts, E. Speiser, J. Räthel, A. Baumann, S. Chandola, and N. Esser, *Phys. Rev. B* **89**, 045313 (2014).
- [28] E. Speiser, N. Esser, S. Wippermann, and W. G. Schmidt, *Phys. Rev. B* **94**, 075417 (2016).
- [29] R. Loudon, *Adv. Phys.* **13**, 423 (1964).
- [30] *Light Scattering in Solids II: Basic Concepts and Instrumentation*, edited by M. Cardona and G. Güntherodt, Topics in Applied Physics Vol. 50 (Springer, Berlin, 1982).
- [31] T. C. Damen, S. P. S. Porto, and B. Tell, *Phys. Rev.* **142**, 570 (1966).
- [32] S. Sanna, S. Neufeld, M. Rüsing, G. Berth, A. Zrenner, and W. G. Schmidt, *Phys. Rev. B* **91**, 224302 (2015).
- [33] M. Veithen, X. Gonze, and P. Ghosez, *Phys. Rev. B* **71**, 125107 (2005).
- [34] J. P. Perdew, K. Burke, and M. Ernzerhof, *Phys. Rev. Lett.* **77**, 3865 (1996).
- [35] G. Kresse and J. Furthmüller, *Phys. Rev. B* **54**, 11169 (1996).
- [36] M. Gajdoš, K. Hummer, G. Kresse, J. Furthmüller, and F. Bechstedt, *Phys. Rev. B* **73**, 045112 (2006).
- [37] G. P. Srivastava, *The Physics of Phonons* (Hilger, Bristol, 1990).
- [38] *Handbook of Optical Constants of Solids*, edited by E. D. Palik (Academic, Orlando, 1998).
- [39] P. A. Temple and C. E. Hathaway, *Phys. Rev. B* **7**, 3685 (1973).
- [40] K. Uchinokura, T. Sekine, and E. Matsuura, *J. Phys. Chem. Solids* **35**, 171 (1974).
- [41] A. Zwick and R. Carles, *Phys. Rev. B* **48**, 6024 (1993).
- [42] N. Esser, K. Hinrichs, J. R. Power, W. Richter, and J. Fritsch, *Phys. Rev. B* **66**, 075330 (2002).
- [43] W. G. Schmidt, S. Glutsch, P. H. Hahn, and F. Bechstedt, *Phys. Rev. B* **67**, 085307 (2003).